Nonlinear analysis of solar cycles

T. Serre[1] and E. Nesme-Ribes[2]

[1] 14, rue Jean Giono, 13 580 La Fare-les-Oliviers, France
[2] Observatoire de Paris, 5 Place Jules Janssen, 92 195 Meudon, France

Abstract. In this paper, the recent improvement of the Wolf sunspot time–series by Hoyt and co-workers has been analysed with the Global Flow Reconstruction (GFR) method (Serre et al. 1996a and b). A nonlinear 4–dimensional chaotic model has been extracted from the data which captures the principal characteristic features of the sunspot group time–series. The hypothesis of interactions between magnetic modes is implicitly tested; presumably, this is the cause of the irregular variations of solar cycle amplitudes recorded since the year 1610. The present results indicate that interactions are occurring between few global magnetic modes.

Key words: chaos – methods: data analysis – Sun: sunspots

1. Introduction

Solar energy variability is one of the possible natural causes of the significant climatic changes reported over past millennia, that cannot be attributed to human effects. In particular, some periods existed in the recent past where the Earth experienced cold excursions (for example, the end of the 16th or the second half of the 17th century), or was warmer than now (the 12nd century).

A decrease of 0.1% of the total solar irradiance is now observed on a 10 yr timescale, i.e. from a solar cycle maximum to the next minimum one (Wilson & Hudson 1988). But it is likely that the sun experienced larger variations. During the 17th century, the solar activity was drastically reduced, and although the solar irradiance was not monitored at that time, it is likely that our Sun showed greater luminosity variations (Nesme–Ribes & Mangeney 1992). This assumption is supported by solar–type stars that also exhibit magnetic cycles accompanied with even larger luminosity variations (up to 2%, Saar & Baliunas 1992). Nesme-Ribes and Mangeney put forward a physical cause for the increase of the number of meridional convective rolls: 1 during the Maunder minimum and 3 at the present time, accordingly the convective velocity decreased from 10 ms^{-1} to 1 ms^{-1}. An estimation of the energy flux E going into large scale motions during a Maunder minimum, is given by

$$E = M_c V_c^2 / \tau_{\mathrm{conv}} \tag{1}$$

where M_c is the mass of the convective roll (10^{31} g), V_c the typical meridional velocity and τ_{conv} the turnover convective time of the order of one year during the Maunder minimum. Note that a reduction of 0.4% of the total solar irradiance was sufficient to produce the little ice–age of the past centuries (Nesme–Ribes et al. 1993). A better understanding of the solar machinery and its output would be a major issue for climate understanding and prediction scenarios.

At one end of the clarification process, the first step is to understand the underlying physics behind the solar cycles (otherwise known as the Schwabe cycles) and its consequence on the solar output. The solar dynamics is certainly a highly complex problem described by a large number of differential equations. However, the principle of normal forms, (Poincaré 1892) and later Ruelle & Takens (1971), shows that if a coupling between the different vibrational modes results through dissipative processes, the dynamics may be confined within a subspace of lower dimension in the state space.

The main question addressed in this paper is to determine whether the dynamics of solar cycles could be of a low dimension. To answer this question, we shall first recall our present understanding of the solar machinery (Sect. 2). Then, using an improved definition of the sunspot number over the last four centuries, we describe and classify the characteristics of solar cycles (Sects. 3, 4). This gives us some indications that solar cycles at a 10 yr timescale may be of low dimension, as reported previously (Ruzmaikin 1981, and especially Spiegel & Wolf 1987, who obtained a geometrical figure similar to an attractor of low dimension). We make use of mathematical tools developed over the last two decades to determine whether the solar cycles can be described as a dynamics of low dimension (Sects. 5, 6). A comparison with other results (Sect. 7) is proposed and followed by a discussion (Sect. 8). This work naturally leads to a prediction of solar activity: this might be proposed in a companion paper.

2. The mechanism driving solar cycles: an alpha-omega dynamo

The solar cycles have a magnetic origin and manifest themselves as sunspots emerging at the solar surface. They are the result of a dynamo process that converts kinetic energy into magnetic en-

ergy taking place at the bottom of the convective zone ($0.7\ R_\odot$ or below). A kinematic description of this dynamo process has been worked out by Parker (1955), the so–called alpha–omega effect, who obtained the magnetic field growth rate from prescribed velocity fields. The latitude distribution of sunspots during solar cycles looks like a butterfly diagram, the higher the extension of the wings, the stronger the cycle (Nesme–Ribes et al. 1994).

The process is nonlinear: magnetic fields influence velocity fields which, in turn, modify the magnetic field growth rate. More recently, extensive numerical simulations of nonlinear dynamos (Brandenburg et al. 1989; Jennings 1991 among others) explored different situations in which the toroidal (sunspot) field could be generated from a dipole (a single magnet roughly parallel to the rotational north–south axis) and from a quadrupole (one magnet per hemisphere). Both dipole and quadrupole modes can be excited in a spherical convective shell, and the competition between the dipole and quadrupole leads to variations of the toroidal field strength, thereby the sunspot number, the sunspot latitude distribution, and their North–South asymmetry distribution. This has been observed (Nesme–Ribes et al. 1994) and would suggest that at least the main characteristics of cycles (strength and duration, as well as longer cycles) could be described by a differential system of low order (at least 3 if the dynamics of the solar cycles is chaotic). These observations and theories naturally lead to this model from the data (this paper and others).

At short timescales sunspot counting looks rather turbulent: sunspot groups appear as bursts of activity every 3 to 5 months, that is, the time for buoyant fields to cross over the convective zone. Furthermore, a hierarchy of velocity fields (from granular motions to higher length scales) is present in the convective zone and certainly partakes in the build-up of the magnetic field. However, we believe that active regions on large length scales (sunspots being part of them) could well be described by the alpha–omega dynamo, and the mean solar cycle, represented by sunspots and active regions, could then be a chaotic nonlinear low dimensional system (see a review on solar variability in Serre & Nesme–Ribes 1997).

3. Sunspot group number (SGN) time series

The best indicator of solar activity is provided by the sunspots because they are the seat of an intense magnetic activity and the poles of the east–west magnets produced by the omega effect. They have been observed with the naked–eye as early as two centuries B.C. in China but since the telescope era (since 1609), they have been carefully monitored. It was only during the mid–19th century it was discovered that the sunspot activity followed a roughly 11 yr cycle. Shortly after, Wolf introduced an empirical indicator, i.e. the sunspot number, that is now currently being used as a solar activity index. The Wolf sunspot number (WSN) is defined as

$$WSN = 10 \times SGN + ISN \times f_c \qquad (2)$$

where SGN is the number of sunspot groups, ISN the number of individual sunspots and f_c a corrective factor for each observer. However, Wolf adopted several simplifications: smoothing monthly fluctuations of sunspots, not using all available archives prior to 1848 and completion of observational gaps by using aurora events as a sunspot index which dangerously mixed two time series of different origins.

Hoyt and co–workers (1992, 1993, 1994) examined again the whole archives, including a complete analysis of 80 yr (8000 data points) of solar observations obtained at the Observatory of Paris, during the 17th century (a work of Nesme–Ribes and co–workers summarized in Nesme–Ribes et al. 1994). This series historically closed the debate in ascertaining the reality of the Maunder minimum (from 1645 to 1705). The improvement by Hoyt and co–workers differs from the Wolf's treatment: they used sunspot group numbers rather than individual sunspots, the new time–series is homogeneous leaving out aurora data and it contains fewer gaps with more than 350 000 observations obtained from more than 350 observers. Also, they used a new approach by normalizing each set of data coming from different observers with the one they considered the best set, i.e. the Royal Greenwich Observatory (RGO) data (1874–1976). The normalizing process can be even more complicated depending on the set considered (see their papers for details). The new SGN time–series is thus more objective, homogeneous and larger than the WSN time–series. A good match between the two time–series is obtained for the well–documented period 1874–1991 after an appropriate scaling (see details in Hoyt et al. 1994): 11.93 multiplies the amplitude of the SGN times–series. Some significant differences with the WSN time–series can be observed near 1750 and also from 1800 to 1848 due to the lack of homogeneity in the WSN time–series.

The leading sunspot of an individual magnet lasts longer than the following sunspots: several days up to one (or exceptionally two) solar rotations for the leading one and, usually less than one rotation for the following one. Therefore, the lifetime of a sunspot group as a whole, is of the order of a solar rotation. So monthly means of the SGN time–series seem to be a good compromise between daily measures and yearly means that do not accurately represent the shape of a solar cycle.

4. Characteristics of solar cycles

On the basis of systematic observations of sunspots available since Galileo's time, certain properties of solar cycles have been derived (Ribes et al. 1987, 1989, 1993). It appears that three types of solar cycles have to be defined (Nesme–Ribes et al. 1994). Let us recall their main properties.

– "**Normal**" cycles: The monthly SGN time–series lies above 8 near sunspot maximum. The cycle length is approximately 10 yr. The latitude distribution (extension of the butterfly diagram) reaches $40°$. The North–South asymmetry in the sunspot production is small.
– "**Weak**" cycles: The monthly SGN time–series lies between 4 and 8 near the time of the maximum. The duration of the

cycle tends to lengthen (up to 13 yr). The latitude distribution does not exceed $30°$. A more pronounced North–South asymmetry in the sunspot distribution is observed.

– "**Maunder minimum type**" cycles: The monthly SGN time–series does not exceed 4. The length is difficult to estimate due to the lack of tracers. The latitude distribution is confined near the equator. A strong North–South asymmetry is observed.

Weak cycles occurred at the beginning of the 18th century and seem to recur every 80 to 100 yr (The Gleissberg cycle). This has been well observed from 1715 onward.

The Maunder minimum, characterized by a drastic lull of solar activity, covered most of the 17th century. Other prolonged grand minima like the Maunder minimum, occurred in the past millenia (Stuiver & Braziunas 1993; Beer et al. 1994). They seemed to last about 100 to 850 yr and recurrence time over the last millenium was every 200 to 400 yr.

There are additional features of solar cycles that have to be considered: the period of rise of solar cycles is usually shorter than the declining phase, leading to an asymmetry in the cycle shape. The asymmetry is usually more pronounced for normal (strong) cycles than for weak ones (Nesme–Ribes et al. 1994).

Our time–series spans almost four centuries. Unfortunately, there are some observational gaps prior to 1749 (with two gaps exceeding 2 yr). So we preferred to restrict our main analysis to the period 1825–1994. Attempts were made by taking account of the 1755 to 1825 data, hoping that we could capture the alternation of weak and normal cycles. In future studies, one could attempt to add the period ranging from 1609 to 1755, in order to include a Maunder type minimum.

5. The reconstruction of the dynamics from data

5.1. Geometric reconstruction of the solar attractor

If the solar activity is a low dimensional chaotic system, one can expect to reconstruct the attractor using the time delay coordinates (Takens 1980; an idea of Ruelle and later extended by Sauer 1994). The knowledge of only one dynamical variable (or a single function of all dynamical variables), in our case the sunspot series, allowed the reconstruction. The dynamical properties of the physical process are preserved because a smooth relation exists between the two state spaces, usually restricted to the attractor region.

If a single, sampled with a fixed time–step, variable $g(t_n)$ is observed (n is an integer labelling the points), one defines the set of d_e–dimensional vectors, called *delay vectors*, $\mathbf{X}^n$ with a time delay τ, as

$$\mathbf{X}^n = (g(t_n), g(t_n - \tau), \cdots, g(t_n - (d_e - 1)\tau)). \quad (3)$$

The new coordinates are simply created by a time shifting of the original signal. It is known from the Whitney's theorem that one can embed a manifold of dimension d in a dimension $2d+1$. In practice, a smaller dimension is often sufficient and the minimum value must be estimated by a trial and error process.

A typical choice for τ is $1/4$ of the main period (11.2 yr for the solar cycle).

5.2. Principles of dynamics reconstruction

The dynamics of the system is supposed to be governed by an O.D.E. of low order d_e (a small set of equations leading to an attractor)

$$d\mathbf{Y}/dt = \mathbf{G}(\mathbf{Y}) \quad (4)$$

where $\mathbf{Y}$ is the d_e–dimensional "state" vector. It is equivalent to describe the system in terms of a stroboscopic sampling $\mathbf{Y}(t_n)$ with successive points linked by a map $\mathbf{F}$ (Takens 1980)

$$\mathbf{Y}(t_{n+1}) = \mathbf{F}(\mathbf{Y}(t_n)). \quad (5)$$

The estimation of the map $\mathbf{F}$ can be done in a *local* way (Farmer & Sidorowich 1988) by an estimation of $\mathbf{F}$ on each subset of a partition of the attractor. If $\mathbf{F}$ is estimated in one piece with the whole attractor, the method is *global* (see a review in Casdagli et al. 1992 and Abarbanel et al. 1993).

A new global method has been developed by Serre et al. (1996a and b), referred to as the *Global Flow Reconstruction*, or GFR, which has already proven to be useful for modelling the behaviour of some irregular pulsating stars (R Scuti in Buchler et al. 1996; AC Herculis in Kolláth et al. 1997). In this paper, we apply the GFR method to the solar sunspot data.

## 6. Application to solar cycles

6.1. The GFR method

The GFR method can only reconstruct a low dimensional dynamics generating a synthetic signal that possesses the same features as the data (Serre et al. 1996a and b). The method is not a mere interpolation process, but it provides a model capturing the dynamics underlying the observations; therefore, it is capable of extrapolation.

The core and originality of the method comes from three combined processes (see tests in Serre et al. 1996a and b). First, a careful data processing is carried out to eliminate spurious behaviours. Second, a robust Singular Value Decomposition (S.V.D., Press & Teutolski 1992) least squares method is used for estimating the coefficients of a nonlinear polynomial expansion of the map. For other types of functions, the reviews of Casdagli (1989) and Weigend & Gershenfeld (1994) should be read. Third, a thorough search of the best model through parameter trials is carried out.

The stability of reconstructed equations needs to be tested by varying the initial conditions for each iteration. A significant set of synthetic signals has to be obtained for a useful covering of the reconstructed attractor. Trials by slightly varying the values of geometric reconstruction parameters, give more precise initial conditions and longer synthetic signals. The possible broadening of the database is another improvement (Farmer & Sidorowich 1988; tests in Serre et al. 1996a and b).
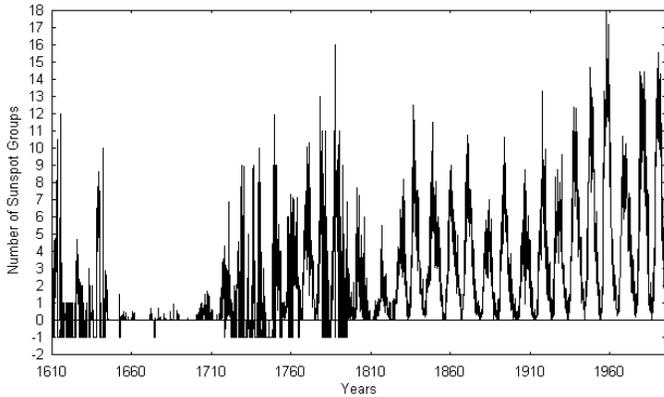
Fig. 1. The original time series of SGN sunspot groups (positive number) and the distribution of gaps (-1 indicates a lack of data)
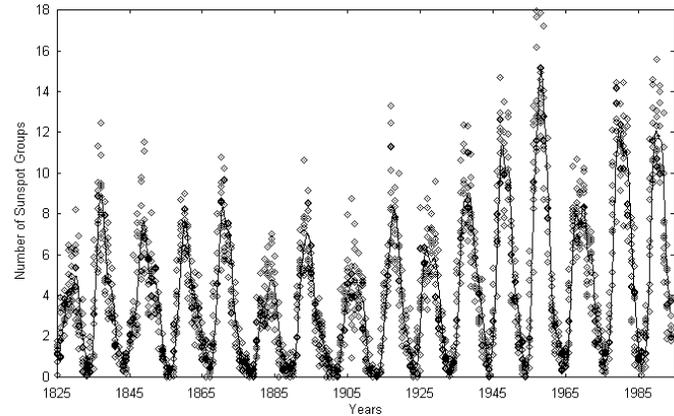
Fig. 2. Global cubic spline smoothing (the continuous line, one knot per original 13 points and modified time–step 0.867 months) together with the original data (dotted diamonds) from 1825 to 1994 (2333 points)

6.2. A fitting of the SGN time–series

Although the SGN time–series covers almost four centuries, the analysis is restricted to the interval 1825–1994 because observational gaps are not present. The data have been smoothed with a time–step of $dt = 0.867$ months, roughly corresponding to a solar rotation and the average lifetime of a sunspot group. Tests confirmed that yearly average would drastically reduce the number of points giving oversmoothed solar cycles, whereas a daily average would contain too large fluctuations. The final value for dt has been adopted by estimating the quality of the synthetic signals obtained from the map for each trial value.

The fitting of the SGN data has been made with cubic spline functions (Press & Teutolski 1992). One advantage of these functions is the possibility of adjusting the nodes at some specific locations in the data and to be able to choose the number of points between the nodes (time–step): a large number of nodes retains information as well as noise, conversely a smaller number of nodes smooths the data. A free time–step is an advantage because the observational timing is not always suitable for a nonlinear analysis. The knots could be chosen arbitrarily, but a straightforward arithmetic averaging in consecutive windows (where knots are the centers) has proven to be sufficient. The polynomials have to ensure that continuity exists on the spline curve and its derivative at each knot.

The effect of the short–term fluctuations on the dynamics, i.e. bursts, is a tricky problem, often encountered in the real world data. Since sunspot counts are used over a well documented period, the observers' errors are negligible compared with the bursts. However, larger fluctuations remain prior to 1825 due to some inaccuracies. Bursts exist in all cycles and they are the results of highly nonlinear magnetic fluctuations which give solar storms. For example, the cycle 6, peaking around 1816 (Fig. 1) has a maximum determined by only four points. Consequently, the smoothed signal appeared to underestimate the maxima. It was obvious that a smooth dynamics could not be responsible for these bursts. The usual straightforward approach was to smooth the bursts and was considered the average dynamics. Therefore, we implicitly adopted the hypothesis of

a *dynamical separation between a low dimensional dynamics and these bursts*.

Lawrence et al. (1995) explored the temporal scale properties of the solar magnetic activity in timescales ranging from days to decades. Applying Haar wavelets to monthly WSN time–series (from 1950 to 1990), they could clearly see two regimes of magnetic activity: first, a generic turbulent structuring results from the rise of magnetic fields through the convective zone implying timescales from 2 days to 2 yr; second, the solar cycle itself (from 6 yr and more). These regimes brought a justification for our data smoothing which eliminated turbulence on short timescales. However, the interaction between these two kind of dynamics is not known with precision in the solar case. Based on this timescale separation, the maxima of Fig. 2 are not underestimated, because they do not correspond to a smooth dynamics. The usefulness of this hypothesis has to be considered with the quality of the results.

WSN time–series was smoothed with a running mean of 13 months that preserved the long–term evolution of cycles but eliminated much of the high–frequency variability. An illustration is found in Mundt et al. (1991): these authors filtered the WSN time–series with a cut–off frequency of $1/6\ \mathrm{yr}^{-1}$, cleaning the time–series, but they got rid of some useful nonlinear properties of solar cycles: a double summit feature at sunspot maximum and a bend in the rising or descending phases of cycles. They did not carry out an error analysis and a broad–band noise should be partially kept because it might correspond to a chaotic dynamical behaviour. Such a simplification could be used for a specific purpose, but it is dangerous with chaotic dynamics.

The spline construction for the data from 1825–1994 was straightforward and made in one piece. In the other hand, the spline smoothing of the 1610–1825 data was harder to work out because of numerous gaps and unobserved data points, so it was left for future works. Not only did splines correctly fit the general properties of solar cycles (lengths and average amplitudes, ensuring the continuity of the curve and its derivatives) but they also kept local features present in the data (double sum-

mits and bends) up to a given degree of smoothness (Fig. 2). The FFTs looked similar between smoothed and original SGN time–series, and solar bursts caused minor differences.

6.3. The construction of synthetic solutions

The time–step and the position of spline knots must be estimated. If the original time–step $dt = 1$ month is kept, the best results for the knot separation are obtained for $dt_k = 8$ to 10 dt and, values from $dt_k = 5$ to 20 dt have usually been tested. If $dt_k < 13\ dt$, the spline approximations preserved the fluctuations whereas, over 19 dt, the signal was oversmoothed. $dt_k = 19\ dt$ was the first knot separation for which the double summit feature was not reproduced. In this case, although the 100 and 11 yr cycles were captured, the forms of the original cycles were not reproduced sufficiently close to the data. Therefore, dt_k has to be less than 19 dt. A progressive increase of dt_k from 10 dt to 19 dt showed that the spline curve smoothed progressively the details of the data. As a trade–off the value $dt_k = 13\ dt$ was chosen.

The original time–step led to synthetic solutions close to the original data, but with systematic small oscillations of the minimum amplitudes which were not a feature of the original data (Fig. 3 top). If dt was increased (decreased), the map was more linear (nonlinear) modifying the ratio between the amplitudes of the frequencies and the harmonics. The best results were obtained with $dt = 13/15$ months (Fig. 3).

Even in the worst cases, some of the features remained captured. Details could be different such as cycle forms and the distribution of high and low amplitude cycles but when the system had been found chaotic, the main features of the data remained showing stability of the reconstructed maps under parameter variations.

At this point, it must be stressed that *for a chaotic system, the synthetic solutions are not expected to be strictly similar to the data* because of sensitivity to initial conditions. Only global characteristics of chaotic systems are retained that are invariant under nonlinear transformations from the real system to the reconstructed one: minimal state space dimension, fractal dimensions of an attractor and, local and maximum Lyapunov exponents (Eckman & Ruelle 1985). However, qualitative comparisons remain possible such as amplitudes and shapes of cycles, the reconstructed attractor shape and FFTs.

Fig. 4 shows the invariant characteristic d_e: the graph of the precision σ of prediction averaged over all the data, one step forward, as a function of the embedding dimension d_e and the order p

$$\sigma = \frac{1}{N}\sum_{i=1}^{N}\sqrt{\frac{1}{d_e}\sum_{j=1}^{d_e}(x_j^{i+1} - F_j(\mathbf{x}^i))^2}. \qquad (6)$$

The prediction precision is not significantly improved for $d_e > 4$. $d_e = 4$ is the minimal embedding dimension for getting synthetic signals close to the data and possibly the true dimension of the dynamics. Although the same precision was obtained for $p = 1$ and $d_e = 6$, i.e. a linear case, the result-
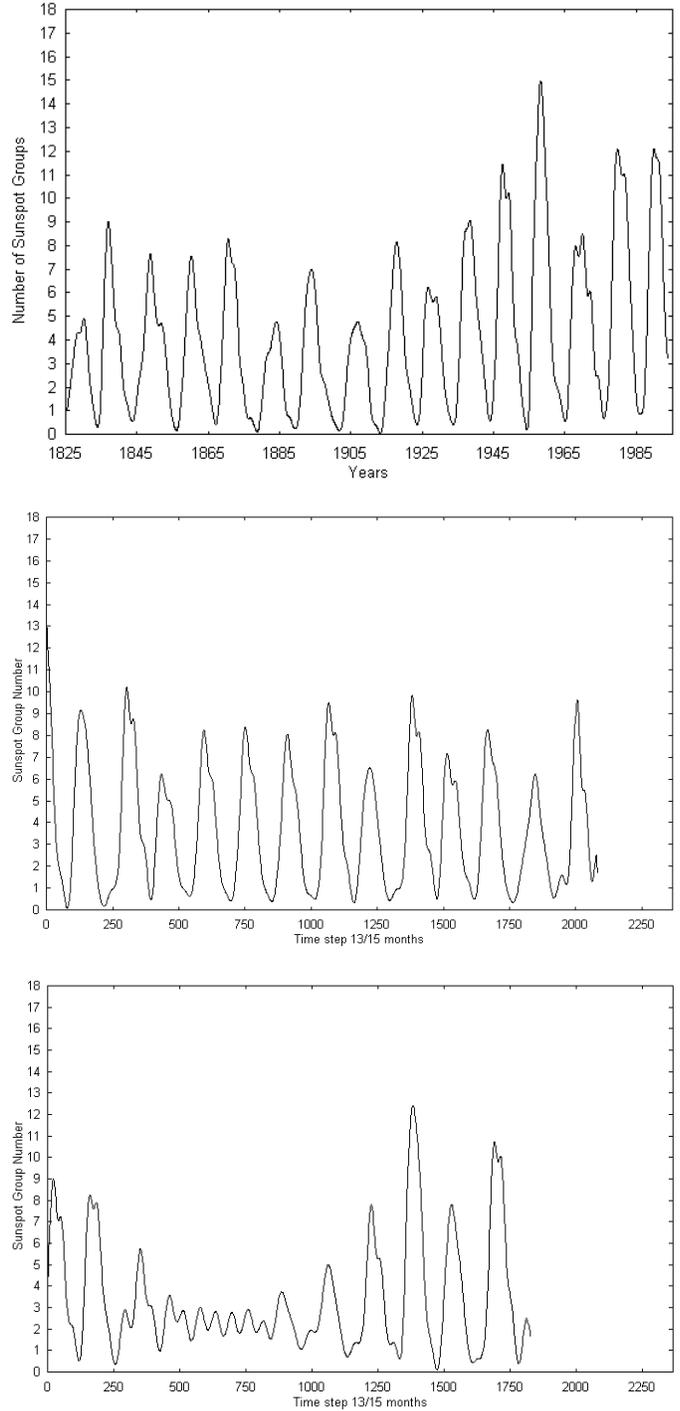
Fig. 3. The original smoothed data are shown on top for comparison. The timescale is the same for the three figures. Two examples of synthetic solutions: without a Maunder minimum (middle), with a Maunder minimum (bottom)

ing synthetic signals never came close to the original data (see Sect. 6.4). Moreover, it is known from applied mathematics that the precision of a fitting process can be increased with a purely linear model in increasing d_e as well as p, but there are no guaranties that the fitted model will give synthetic solutions similar to the data: the gain in precision is only local for a map. There-
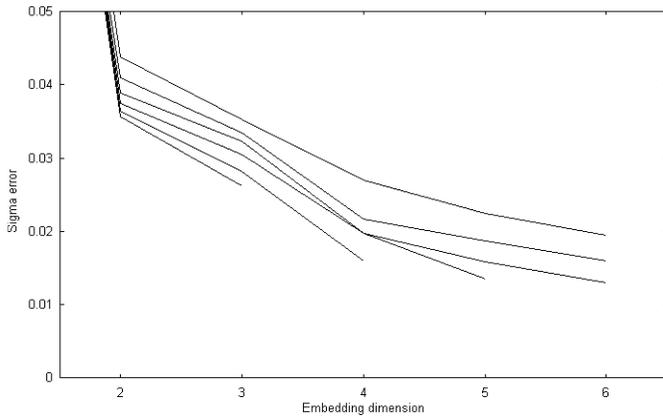
Fig. 4. Error norm σ as a function of the embedding dimension d_e and the polynomial order, $p = 1$ to 6, increasing from top to bottom

Table 1. The 73 synthetic solutions found longer than 6.45 solar cycles. All the 2306 available initial conditions have been tested for the data from 1825 to 1994. (a) is a solution with 2080 points (149.76 yr or 13.37 solar cycles)

Range(pts)	Size(yr)	Cycles	
1000–1200	72.20–86.60	06.45–07.73	37
1200–1400	086.60–101.10	07.73–09.03	22
1400–1600	101.10–115.50	09.03–10.31	09
1600–1800	115.50–129.60	10.31–11.57	01
1800–2000	129.60–144.00	11.57–12.86	03
> 2000	> 144	> 12.86	1 (a)

fore, the estimation of d_e is not sufficient for chosing the right model.

6.4. Results

By changing the embedding dimension d_e and the nonlinear order p, we obtained the following results. For $p = 4$ and 5, the synthetic solutions were essentially identical. On the other hand, for a nonlinear order less than $p = 4$, no solutions came close to the data. For $d_e = 1$ or 2, no physical solutions were possible (crossings of trajectories in the state space). If $d_e = 3$ and p up to 6 no solutions approached the data. The best synthetic solutions corresponded to $d_e = 4$, $p = 4$ with a delay $\tau = 9\ dt$ (7.8 months).

It was necessary to get synthetic signals with enough cycles to calculate the characteristics of chaotic dynamics and get Maunder minimum events. However, the synthetic chaotic solutions has never been iterated beyond 149.76 yr in a single run. Another strategy had to be used to get more of the longer solutions. All the available initial conditions (Table 1) were used for producing 2306 solutions. No longer solutions had been found but a better covering of the attractor was obtained with shorter ones. Solutions presenting periods similar to a Maunder minimum event occurred by way of this method. Neither an increase of the time–step, nor other parameter changes seemed to improve the number of longer solutions. Indeed, it is well known that an increase in the number of cycles in the database will be necessary to improve the stability of synthetic solutions. This has not been possible with the low quality of the remaining sunspot data.

The solution with the maximum length (149.76 yr) as well as a solution presenting a Maunder minimum (132.05 yr) shown in Fig. 3, are the most representative solutions for comparison with the data, therefore they shall be discussed.

A comparison between Fig. 3 (top) and Fig. 3 (middle and bottom) shows a qualitative similarity between the original data and the synthetic solutions (same period of 2333 $dt =$ 2022.71 months). Double maxima are reconstructed with variations in amplitudes. The asymmetry of the ascending and de-

scending branches, as well as minima with a little hump are captured. The three types of cycles (normal, weak, Maunder minimum) are present, but the small cycles inside the Maunder minimum do not exist in the original data (Fig. 3 bottom). Another important feature is reproduced: the larger the amplitude cycle the smaller the cycle duration.

Although a chaotic dynamics does not allow a comparison point by point, it is interesting to note that some synthetic cycles are very close to real cycles (consider matching cycles on top of Fig. 3 with those in the middle and bottom).

Fig. 5 shows geometrical figures reconstructed with the time delay method in a 4–dimensional state space for the signals shown in Fig. 3. Although only qualitative conclusions can be drawn from 4–dimensional projections (unless specific multi-dimensional analysis methods could be used), both general features as well as important details seem to be captured. The Lyapunov exponent estimations in Sect. 6.5 indicate that the figures in Fig. 5 display an attractor, i.e. a subspace attracting trajectories. The flat parts correspond to ascending branches of cycles; the curved parts correspond to descending branches; the little swerves are double summit features as well as inflections at the bottom of cycles. Larger amplitude cycles are not shown in the figures of Fig. 3 (middle), although they exist in other signals and in Fig. 3 (bottom).

The envelope and the main locations of frequency powers are reproduced in the power spectrum. However, as expected, the Maunder minimum case is different with respect to a solution without one. In the latter case, amplitudes of frequency harmonics are increased whereas amplitudes of low frequencies are decreased, especially the main group of power centered on 11.2 yr period (0.089 yr^{-1} frequency): the dynamics is more nonlinear.

The surprising property of the dynamics is that it produces Maunder and Dalton type minima (Fig. 3 bottom) while there are no such events in the data from 1825 to 1994. It seems therefore that the data from 1825 to 1994 contain partial information on the Maunder minimum: Fig. 2 shows cycles approaching minima, i.e. Gleissberg events around 1885 and 1970 but with higher amplitudes than the Maunder minimum of the 17th century. Therefore, the attractor is incompletely explored near the region of the minima. The minima found on synthetic solutions display periodic cycles at a mean level 2 which is higher than the
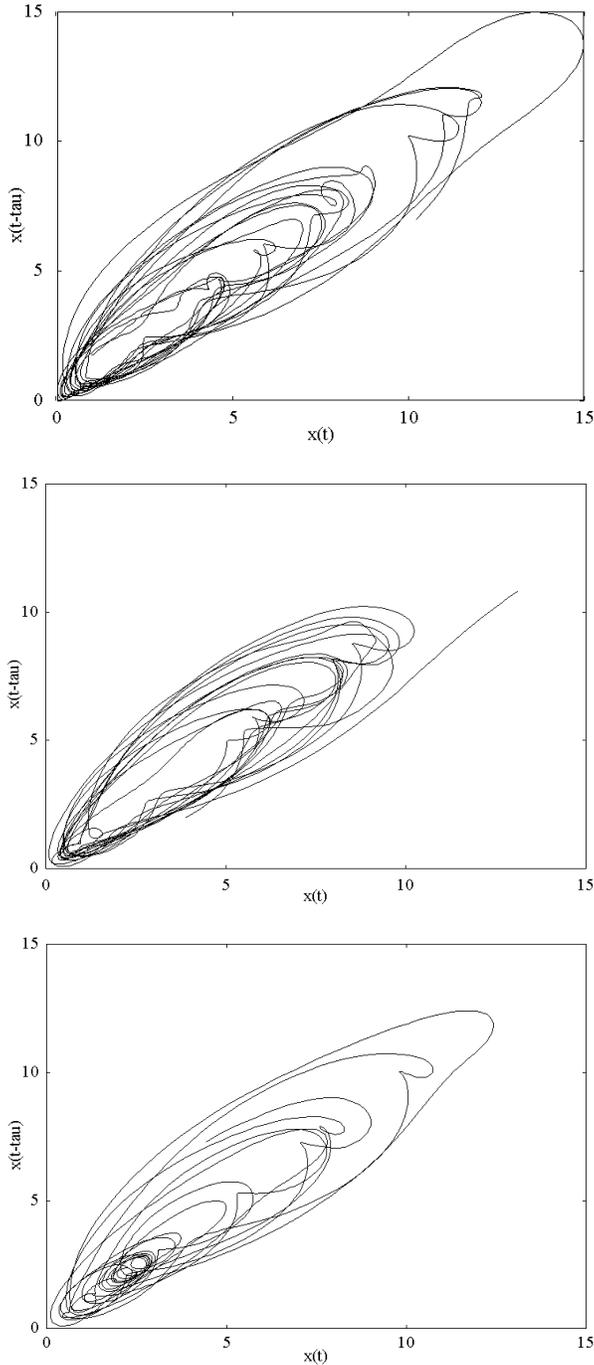
Fig. 5. Projections in 2D of the 4–dimensional space where the synthetic solutions of Fig. 3 are embedded with the time delay method: a part of the real spline smoothed data of Fig. 3 (top), synthetic solutions without a Maunder minimum (middle) and with a Maunder minimum (bottom)

level of the historical Maunder minimum. The quasi–periodic behaviour reconstructed inside the synthetic minimum in Fig. 3 (bottom) should not be taken as real since the information was not initially present in the data, i.e. the sunspots were almost not present during the historical Maunder minimum (Fig. 1).

Several attempts were made to include more cycles prior to 1825. However, the low quality of these data did not allow us to get solutions, only flat lines were obtained. A rough spline smoothing adding only the Dalton minimum (1811–1825) showed that solutions close to the data were obtained with $d_e = 4$, $p = 4$ and $\tau = 9$ dt. Again the reconstructed map lacked stability under iteration and no more than 163.6 yr had been found in a single run. Maunder minimum type events were closer to the zero level (about 1.5). Unfortunately, the rate of occurrence of Maunder type minima (see an estimation in Sect. 6.5.3) was not consistent with the estimation of Kurths et al. (1996) which was an indication that the reconstructed dynamics was partially different from the real one. However, if the nature of the dynamics is *chaotic intermittency*, as is suspected for solar cycles, it is well known that the efficiency of the trajectory trapping mechanism is sensitive to the reconstruction process affected by the lack of data (only 15 solar cycles really usable) and could explain the difference.

6.5. Additional tests

6.5.1. Principle of the Lyapunov exponent estimations

Lyapunov exponents estimate the average divergences of infinitesimal volumes inside an attractor. If at least one Lyapunov exponent is positive, a dynamical system is chaotic (Eckman & Ruelle 1985; Bergé et al. 1984 for general notions on chaos). The estimation of the spectrum of Lyapunov exponents ($\lambda_i, i \in \{1, \cdots, d_e\}$) consists of analysing the exponents of the matrix resulting from the multiplication of L successive local tangent matrices. They are called *local* if L is finite, otherwise they are the *maximum Lyapunov exponents*. Local Lyapunov exponents are dependent on locations inside the attractor, therefore they are not invariant under smooth nonlinear transformations and not representative of the dynamics **F**. But an averaged quantity over the attractor is a dynamical invariant. This is the case for Lyapunov exponents obtained by space averaging (dependence only in L). Moreover, $\lambda_i(L)$ measures the prediction efficiency for a given L and this particular exponent.

$$\lambda_i(L) = \int \rho(\mathbf{X0})\lambda_i(\mathbf{X0}, L)d\mathbf{X0} \qquad (7)$$

$$\sigma_i(p, L) = \int \rho(\mathbf{X0}) \mid \lambda_i(\mathbf{X0}, L) - \lambda_i(L) \mid^p d\mathbf{X0} \qquad (8)$$

where $\sigma_i(p, L)$ are the moments of order p about the average and ρ is a physical measure (equal to the δ distribution in physics). σ is useful in prediction applications because this is the mean dispersion of the divergence for a given L, giving a picture of the most divergent parts in the attractor (Abarbanel et al. 1991).

An estimation of the dimension of the dynamics d_L, i.e. the Lyapunov dimension, is given by using the Kaplan–Yorke conjecture (Kaplan & Yorke 1979)

$$d_L = k - \frac{\sum_{\alpha=1}^{k} \lambda_\alpha}{\lambda_{k+1}} \qquad (9)$$

where k is the number of Lyapunov exponents added together giving a positive sum. Better dimension estimations are obtained with large L values because more precise Lyapunov exponents are estimated.

6.5.2. Results

All our models are too unstable for displaying sufficient long runs of synthetic signals allowing reliable maximum exponent estimations. But following Abarbanel et al. (1991), this problem was dealt with the estimation of the local Lyapunov exponents, the distribution and evolution following L, and the asymptotic values. The hypothesis is that $\sigma_i(p, L)$ and $\lambda_i(L)$ are described by the following power laws

$$\sqrt{\sigma_i(2, L)} = a_i L^{-\nu_i} \tag{10}$$

$$\lambda_i(L) = \lambda_{i,\max} + C_i L^{-\nu_i}. \tag{11}$$

ν_i depends only on the dynamical system ($0.5 \leq \nu_i \leq 1$) and, C_i and a_i are constants determined by the dynamics. Fig. 6 and Fig. 7 use the linear laws from Eqs. (12) and (13) respectively.

$$\lambda_i = \lambda_{i,\max} + \frac{c_i}{a_i} \sqrt{\sigma_i(2, L)} \tag{12}$$

$$\log \sqrt{\sigma_i(2, L)} = -\nu_i \log L + \log a_i. \tag{13}$$

These laws are adjusted to the data by a least square process. Eq. (12) is used to estimate the maximum Lyapunov exponent $\lambda_{\max}$ (the most positive one).

The results, sumarized in Tables 2, 3 and 4, confirm that the Lyapunov exponents follow a power law for the values and the RMS distributions (Fig. 6 and 7). After about two orbits (310 points), no significant improvements are detected. If 1000 points are taken to carry out the averaging, the results remain similar. Therefore, fewer points can be used without altering the averaging after one orbit. The first point ($L = 1$) is not used in the linear fitting of the Eqs. (12) and (13), because the estimations with short L values are much less precise. However, λ_4 and $\sigma_4(2, L)$ do not obey the same law. An explanation is that there is a lack of information about converging trajectories towards the attractor, measured by the most negative exponent, which does not allow an efficient averaging. It is well known from numerical experiments on dynamical systems that the most negative exponents are quite sensitive to noise and all kinds of uncertainties (Abarbanel et al. 1991). However, the Lyapunov dimension has always been found between 3 and 4 whatever the outcome of our experiments (Table 3 and the estimation of the power laws in Table 4). The volume variation, given approximately by the sum of the Lyapunov exponents, is always negative confirming an expected contraction of volumes near a dissipative chaotic attractor.

An estimated value of the Lyapunov dimension, based on the estimated power laws (Table 4), gives $d_L = 3.12$ with the maximum of averaging points (variable following L) and $d_L = 3.34$
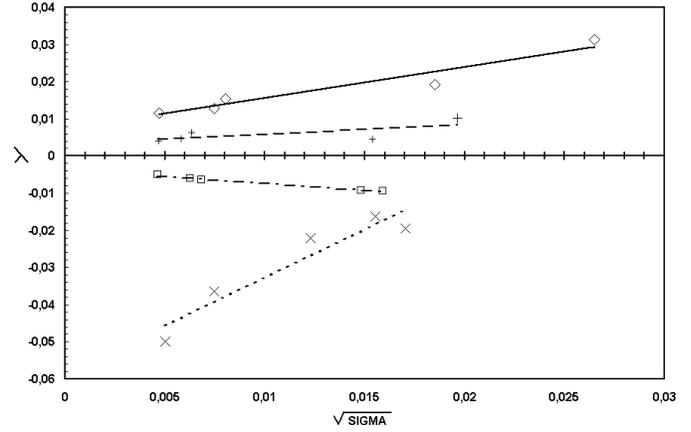
Fig. 6. Data and linear fits of the averaged local Lyapunov exponents following $\sqrt{\sigma_i(2, L)}$ dispersions. λ_1 is the thick line with the 'diamond' data, λ_2 the large dashed line with the 'plus' data, λ_3 the dotted–dashed line with the 'square' data and λ_4 the dotted line with the 'cross' data. The fitted laws are given by the Eq. (12)
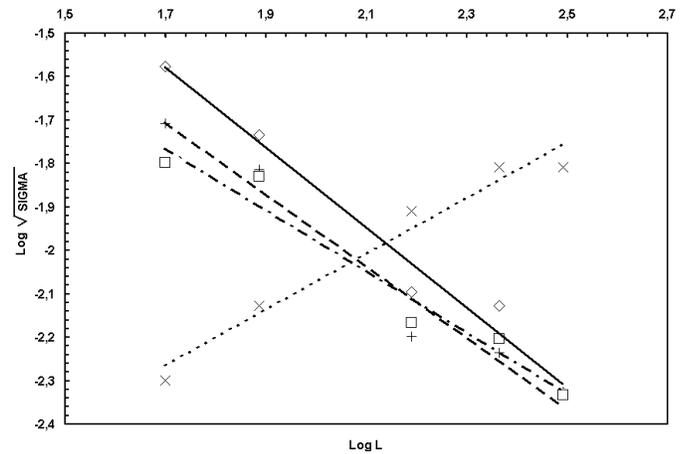
Fig. 7. Data and linear fits of the local Lyapunov exponent dispersion $\log \sqrt{\sigma_i(2, L)}$ following $\log L$ iterations (same codes as in Fig. 6). The fitted laws are given by the Eq. (13)

for exactly 1000 averaging points for all L values (homogeneous statistics). Therefore, the dynamics is fractal and at least 4 variables are necessary to describe it.

The maximum Lyapunov coefficient is around $6.5 \, 10^{-3}$ per month (averaged between the case (a) and (b) in Table 4). This value leads to an averaged increase of initial errors by a factor of 10 for 200 iterated points (1.3 orbits). If A is the mean size of an attractor in the state space, Z an Euclidean length for an initial error and t_g the time of growth of the initial uncertainty, the following relation holds

$$t_g \approx \frac{|\log(A/Z)|}{\lambda_{\max}}. \tag{14}$$

Therefore any prediction capability is theoretically wiped out (a total loss of information) in about 2.4 orbits if $A = 14$ and $Z = 0.1$ (About 5.6 orbits for $Z = 10^{-4}$). However, the prediction time limit is only an average and the prediction is

Table 2. Local Lyapunov exponents for data between 1825–1994. All estimations are made over 2306 time delay vectors of the database for the case $d_e = 4$, $p = 4$, $T = 9\ dt$ (The values in the second column are in $13/15\ \mathrm{month}^{-1}$ units)

Number	Value	$\sqrt{\sigma(2, L)}$	Points
1 iteration			
λ_1	$1.11\ 10^{-1}$	$1.981\ 10^{-2}$	2279
λ_2	$5.718\ 10^{-2}$	$3.267\ 10^{-2}$	2279
λ_3	$-2.051\ 10^{-2}$	$2.547\ 10^{-2}$	2279
λ_4	$-1.51\ 10^{-1}$	$2.867\ 10^{-2}$	2279
50 iterations			
λ_1	$3.130\ 10^{-2}$	$2.648\ 10^{-2}$	2192
λ_2	$1.023\ 10^{-2}$	$1.962\ 10^{-2}$	2192
λ_3	$-9.447\ 10^{-3}$	$1.592\ 10^{-2}$	2192
λ_4	$-4.992\ 10^{-2}$	$5.018\ 10^{-3}$	2192
77 iterations			
λ_1	$1.927\ 10^{-2}$	$1.850\ 10^{-2}$	2113
λ_2	$4.586\ 10^{-3}$	$1.539\ 10^{-2}$	2113
λ_3	$-9.219\ 10^{-3}$	$1.481\ 10^{-2}$	2113
λ_4	$-3.650\ 10^{-2}$	$7.447\ 10^{-3}$	2113
155 iterations			
λ_1	$1.542\ 10^{-2}$	$8.045\ 10^{-3}$	1438
λ_2	$6.235\ 10^{-3}$	$6.344\ 10^{-3}$	1438
λ_3	$-6.461\ 10^{-3}$	$6.825\ 10^{-3}$	1438
λ_4	$-2.216\ 10^{-2}$	$1.230\ 10^{-2}$	1438
232 iterations			
λ_1	$1.282\ 10^{-2}$	$7.466\ 10^{-3}$	1203
λ_2	$4.778\ 10^{-3}$	$5.811\ 10^{-3}$	1203
λ_3	$-6.057\ 10^{-3}$	$6.245\ 10^{-3}$	1203
λ_4	$-1.952\ 10^{-2}$	$1.554\ 10^{-2}$	1203
310 iterations			
λ_1	$1.153\ 10^{-2}$	$4.713\ 10^{-3}$	979
λ_2	$4.109\ 10^{-3}$	$4.659\ 10^{-3}$	979
λ_3	$-5.005\ 10^{-3}$	$4.617\ 10^{-3}$	979
λ_4	$-1.634\ 10^{-2}$	$1.554\ 10^{-2}$	979

Table 3. Estimation of the Lyapunov dimension (d_L) for a given L and the sum of the Lyapunov coefficients (ΔV) linked to the infinitesimal volume variations. The second column gives the number of points used for the averaging

L	points	d_L	ΔV
1	2279	3.98	$-3.300\ 10^{-3}$
50	2192	3.64	$-1.779\ 10^{-2}$
77	2113	3.40	$-2.186\ 10^{-2}$
155	1438	3.68	$-6.966\ 10^{-3}$
232	1203	3.59	$-7.979\ 10^{-3}$
310	979	3.65	$-5.706\ 10^{-3}$

degraded well before the theoretical limit because the initial error Z is only a few percent of the amplitude.

One of the Lyapunov coefficients has to be zero. This is the nondivergent direction, i.e. tangent to the trajectory. The second and third coefficient seem to be nearest to the zero value. It is hard to tell which one is closer, but the two are small, therefore

Table 4. Parameters of the Least squares fitting of the Eqs. (12) and (13) with the maximum number of points (a) and 1000 points for all averages (b)

	λ_1	λ_2	λ_3	λ_4
a(a)	0.974	0.508	0.276	$4.35\ 10^{-4}$
a(b)	0.848	0.624	0.261	$2.95\ 10^{-4}$
ν (a)	0.922	0.829	0.709	-0.666
ν (b)	0.890	0.876	0.695	-0.734
C (a)	0.816	0.134	-0.103	$1.13\ 10^{-3}$
C (b)	0.892	0.303	-0.067	$-3.66\ 10^{-4}$
λ_{max} (a)	$7.1\ 10^{-3}$	$3.3\ 10^{-3}$	$-3.6\ 10^{-3}$	$-5.86\ 10^{-2}$
λ_{max} (b)	$5.9\ 10^{-3}$	$2.5\ 10^{-3}$	$-4.3\ 10^{-3}$	$-1.22\ 10^{-2}$

the dynamics remains dominated by only the largest positive exponent: *the very sign of a chaotic dynamics*. This uncertainty gives a large estimation of the error on the Lyapunov exponents: on average between the case (a) and (b) of the Table 4, the error is $\Delta\lambda = 3.5\ 10^{-3}$ (a) and $3\ 10^{-3}$ (b). Based on these errors, an error estimation for d_L gives $\Delta d_L = 0.19$(a) and 0.6 (b). We think that this estimation is too large, because the value and error on λ_4 is not known with precision. Therefore, a large uncertainty remains on the value of d_L, but since λ_4 is usually more negative than our estimation, we are confident for $3 < d_L < 4$.

By adding the data from 1811 to 1825, the Lyapunov exponents and corresponding power laws are not significantly affected. The power laws for the most positive exponent become

$$\sqrt{\sigma(2, L)} = 0.984\ L^{-0.815} \tag{15}$$

$$\lambda(L) = 1.317\ 10^{-2} - 3.749\ 10^{-2} L^{-0.815} \tag{16}$$

with $\nu = 0.815$ and a maximum Lyapunov exponent $\lambda_{max} = 1.317\ 10^{-2}$. This estimation holds for $L = 50$ and $L = 155$ iterations.

6.5.3. Occurrence of the Maunder minima

Kurths et al. (1996) made a detailed analysis of the occurrence of the Maunder minima in radio carbon data of Sonnet (1992) from 5884 B.C. to 1886 A.D. This analysis furnished a way to check our model. Therefore, their method for choosing a Maunder minimum has to be followed.

A sliding linear averaging window of ± 30 yr has been applied for decreasing the amplitude of the high frequency noise. They considered that a Maunder minimum was detected if the average amplitude was less than a chosen value and the period of the minimum was above about 25 yr (about 2 solar cycles). They tested the robustness of their results against parameter variations. They found a good correspondence with the historical sunspot data with only 34 grand minima over a 7750 yr period (a frequency of 4.38 minima for 1000 yr). Statistical estimations gave a 61 yr mean duration of grand minima (shortest 30 yr, largest 135 yr). They noted that the succession in time appeared random (see their Fig. 21).

Table 5. Maunder type minima found with the GFR model applied on the SGN time–series, based on the criterion of Kurths et al. (1996)

First(yr)	Amplitude	Size (yr)	Solar cycles
1835.46	2	38.28	3.48
1835.48	4/4	34.67/41.89	3.15/3.81
1850.77	4.5	23.83	2.16
1872.87	4.75	22.39	2.03
1880.38	3.5/5	31.05	2.82
1920.11	4.25	21.66	1.97
1928.12	4.75	21.67	1.97
1959.61	4.75	34.67	3.15

In the original data set, we have chosen a grand minimum amplitude of 5 for accepting a minimum event in the synthetic data because of the Dalton and 1900 minimum amplitude. Since a very large single run was not available, the longest possible runs had to be chosen. There are 18 initial conditions with more than 1300 points iterated. The resulting total period of the minimum events is 128.6 yr over 2100.87 yr iterated with 9 grand minima identified with sizes more than 2 solar cycles (Table 5). The result is 4.28 grand minima per 1000 yr which is a satisfactory close value to that of Kurths et al.. But we found only a 30.01 yr mean duration of grand minima, less than half Kurths et al.'s result. This is probably the result of a statistical lack of grand minima because the uniform covering of our attractor is not secured. Therefore, these results are only an indication of the quality of our model. The case with the Dalton minimum added, showed 8.99 minima per 1000 yr which indicated that the state space part leading to grand minima was too attractive. Adding more cycles to the database would certainly improve the result.

7. Comparisons with other methods of signal analysis

An earlier attempt to predict the solar cycle was carried out by Yule (1927) with an *ARMA stochastic* method, since then, the study of the ARMA type prediction methods has developed an important domain of applied mathematics. However, the results were not satisfactory for solar cycles because the strong asymmetry of the cycle shape could not be reproduced and predictions were only made on short periods (less than several years). Better forecasts were obtained with the use of *stochastic nonlinear models* based on a state space representation (Tong & Lim 1980).

An interesting study has been done on solar predictions allowing a comparison with our results. Using monthly WSN time–series from 1750 to 1990, Mundt et al. (1991) studied the dimension of the suspected solar sunspot chaotic system. They adopted the local method of Farmer and Sidorowich (1988), already used for the purpose of sunspot data prediction (see a review of Casdagli et al. 1992). They explored a large range of embedding dimensions (2 to 10) and time delays. They used the fractal dimension estimation method (Eckman & Ruelle 1985). A rough limit for this method has been given by Ruelle (1990): the upper bound for the dimension is usually $2 \log_{10}(N)$ with

N the number of points: in this paper, the limit in dimension is 6.7 for the sunspot data. They chose a time delay of 10 months, comparable to ours, and found an embedding dimension of 3. However, a severe criticism to Mundt et al.'s work applies to their analysis of the signal. They used yearly WSN time–series for the period 1750 to 1990 applying a severe cut–off frequency of $1/6$ yr^{-1}. The danger in adopting a too strong smoothing is that important information can be missed (Serre et al. 1996a and b; Buchler et al. 1996). If a spline smoothing with 1 knot per 19 months is adopted for our model, corresponding to Mundt et al.'s choice, important details of the sunspot data are over-smoothed. Their embedding dimension of 3 might simply reflect the severe frequency cut–off. In our paper, the data have been more carefully smoothed.

Ohtomo et al. (1994) produced a Maximum Entropy (MEM, Press & Teutolski 1992) analysis of solar cycles. They made the serious claim that *the solar activity was regular and predictable (quasi–periodic)* with 5 frequencies! This was clearly a bold claim, obviously not supported after almost one century of research. Their model did not reproduce well the form of the cycles, especially the highly asymmetric ones. Interestingly, predictions inside the known signal were not really successful, whereas a quasi–periodic dynamics is expected to be highly successful, especially with 5 frequencies. The remaining fluctuating part in the MEM spectrum cannot be discarded easily.

What was common among all the studies mentioned above (including ours) was that the mean solar cycles had been assumed to be described by a small number of differential equations or maps. The claimed value 3 for the state space dimension was probably caused by a drastic smoothing of the WSN time–series. The signal processing plays thus a crucial role.

In contrast with most *local* models, the GFR method is concerned with the attractor, considered as a whole. The underlying assumption remains that the system is weakly nonlinear and the local behaviour can be described by a polynomial expansion (a reasonable hypothesis). Moreover, piecewise linear maps do not allow for a direct global physical insight, because a low dimensional dynamics is presented as a collection of maps whereas global methods furnish a unique model more closely related to the dynamics, therefore easier to consider (Sect. 3 in Casdagli 1989).

8. Discussion and conclusion

Using the SGN time–series as an index of the toroidal magnetic field, over the period 1825–1994, we found that the average solar cycle could be described by a 4D differential system. The results of papers reporting an embedding dimension of 3 are not supported by the present analysis. This result was established by an analysis of the data with the GFR method. Other objections and discussions have been raised (Perdang & Serre 1998; Spiegel 1997) especially concerning the nature and impact of the solarlike turbulence.

The embedding dimension 4 for the SGN data is the minimum found with the GFR method. The particular value of the nonlinear degree is not crucial since the theoretical value is in-

finite (polynomial expansion). We showed that events similar to the Maunder and Dalton features occurred in our synthetic curves. Such a dynamical lull exists in non chaotic dynamics but it requires a large number of oscillating modes. Stochastic dynamics could produce low amplitude cycles but our result has given the alternative of a low dimension dynamics. The presence of several coexistent attractors in a state space could also explain the result but we could not check this alternative since a full knowledge of the state space is required. One of these cases is the intermittent chaotic dynamics discovered in the beginning of the eighties (Pommeau & Manneville 1980). Such a dynamics could be tested if bifurcations, obtained with parameters variations of the solar physical dynamical system, had been possible.

A solution of the mean field dynamo, with truncated equations, has been obtained presenting an intermittent chaos called crisis–induced intermittency (Covas & Tavakol 1997). This is the first time that such a chaos has been identified in the dynamo equations suggesting that this dynamics could be present in stellar dynamos. The dynamics displays variable behaviours showing alternating temporal evolution between two close chaotic attractors. Therefore, a theoretical support exists for the intermittency interpretation of the Maunder and Dalton minima.

The analysis of Kurths et al. (1996) of the distribution of lengths of the Maunder minima does support an intermittent dynamics derived from C^{14} data (Sonnet 1992). Their distribution is similar to the one of type III intermittency, i.e. the maximum number of lengths of Maunder minima occurs for the smaller lengths. Unfortunately, a signal processing of data with more solar cycles will be necessary in order to establish such a distribution with the GFR method.

Our results are consistent with computer models of the solar dynamo. According to these models, the competition between dipole and quadrupole modes of the overall magnetic field drives the solar cycles. Indeed, a major question is why there are shifts between weak and strong cycles. In the framework of the nonlinear dynamo theory, a solution, referred to as the mixed parity mode, occurs when both dipole and quadrupole are weak and of equal intensity (Brandenburg et al. 1989; Jennings 1991; Sokoloff & Nesme–Ribes 1994). Such a mode leads to weak solar cycles, possibly corresponding to Maunder minima. Strong (chaotic) cycles would correspond to a dominant dipole field. On the other hand, the competition between dipole and quadrupole modes could also be controlled by the highly turbulent convective zone in a stochastic dynamics, i.e. a high dimension dynamics advocated by Spiegel (1997). It must also be stressed that nonlinear couplings between two modes could be sufficient to lead to a complex behaviour of solar cycles and are supported by the present results. However, the validity of our results was established for the data we used. Long term stochastic effects could not be ruled out, changing the characteristics of the dynamics, and certainly deserve future studies.

References

Abarbanel H.D., Brown R., Kadtke J.B., 1991, Physical Review A 41, 1782

Abarbanel H.D., Brown R., Sidorowich J.J., Tsimring T.S., 1993, Rev. Mod. Phys. 65, 1331

Beer J., Joas F., Lukasczyk C., et al., 1994, 10Be as an Indicator of Solar Variability and Climate, in: Nesme–Ribes E. (ed.) NATO ASI Series I 25, The Solar Engine and its Influence on the Terrestrial Atmosphere and Climate, Berlin: Springer, p. 221

Bergé P., Pommeau Y., Vidal C., 1984, The Order in Chaos. New York: Wiley

Brandenburg A., Krause F., Meinel R., Moss D., Tuominen I, 1989, A&A 213, 411

Buchler J.R., Kolláth Z., Serre T., Mattéi J., 1996, ApJ 492, 489

Casdagli M., 1989, Physica D 35, 335

Casdagli M., Des Jardins D., Eubank S., et al., 1992, Nonlinear Modeling of Chaotic Time Series: Theory and Applications, in: Kim J.H., Stinger J. (eds.), Applied Chaos. New York: Wiley, p. 335

Covas E., Tavakol R., 1997, Physical Review E 55, 6641

Eckman J.P., Ruelle D., 1985, Rev. Mod. Phys. 57, 617

Farmer J.D., Sidorowich J.J., 1988, Exploiting Chaos to Predict the Future and Reduce Noise, in: Lee Y.C. (Ed.), Evolution and Learning and Cognition. World Scientific, Singapore, p. 277

Hoyt D., Schatten K.V., 1992, Solar Physics 138, 387

Hoyt D., Schatten K.V., Nesme–Ribes E., 1993, J. Geophys. Res. Letters 21, 2067

Hoyt D., Schatten K.V., Nesme–Ribes E., 1994, A New Reconstruction of Solar Activity, 1610–1993, in: Nesme–Ribes E. (Ed.), NATO ASI Series I 25, The Solar Engine and Its Influence on the Terrestrial Atmosphere and Climate. Berlin: Springer, p. 57

Jennings R.L., 1991, MNRAS 252, 249

Kaplan J.L., Yorke J.A., 1979, Lecture Notes in Mathemathics 730, 228

Kolláth Z., Buchler J.R., Serre T., Mattéi J., 1997, A&A 329, 147

Kurths J., Feudel U., Jansen W., Schwarz U., Voss H., 1996, Solar Variability: Simple Model and Proxy Data, in: Cini C., Provenzale A. (Eds.), Proc. International School of Physics 'Enrico Fermi' course CXXXIII, Solar Variability: Simple Models and Proxy Data, Varenna

Lawrence J.K., Cadavid A.C., Ruzmaikin A.A., 1995, ApJ 455, 366

Mundt M.D., Maguire II W.B., Chase R.R.P., 1991, J. Geophys. Res. 96 A2, 1705

Nesme–Ribes E., Ferreira E., Sadourny E.N., Le Treut R., Li L., 1993, J. Geophys. Res. 98 A11, 18923

Nesme–Ribes E., Mangeney A., 1992, Radiocarbon 34 2, 263

Nesme–Ribes E., Sokoloff D., Ribes J.C., Kremliosky M., 1994, The Maunder Minimum and the Solar Dynamo, in: Nesme–Ribes E. (Ed.), Proc. NATO ASI Series I 25, The Solar Engine and Its Influence on Terrestrial Atmosphere and Climate. Berlin: Springer, p. 71

Ohtomo N., Saburou T., Tanaka Y., Tokiwano K., Kaneko N., 1994, Japan J. Appl. Phys. 33, 2821

Parker E.N., 1955, ApJ 122, 239

Perdang J., Serre T., 1998, A&A 334, 976

Poincaré H., 1892, New Methods of Celestial Mechanics. New York: American Institute of Physics (1993)

Pommeau Y., Manneville P., 1980, Commum. Math. Phys. 74, 189

Press W.H., Teutolski S.A., 1992, Numerical Recipes, Cambridge: University Press

Ribes J.C., Ribes E., 1993, A&A 276, 549

Ribes E., Ribes J.C., Barthalot R., 1987, Nature 326, 52

Ribes E., Ribes J.C., Merlin Ph., Barthalot R., 1989, Annales Geophysicae 7, 321

Ruelle D., 1990, Proc. R. Soc. London, Series A 427, 241

Ruelle D., Takens F., 1971, Commun. Math. Phys. 20, 167

Ruzmaikin A.A., 1981, Comm. Astrophys. 9, 85

Saar S., Baliunas S.L., 1992, Starspot Cycles, in: Harvey K.L. (Ed.), Proc. ASP Conf. Ser. 27, The Solar Cycle, p. 150

Sauer T., 1994, Time Series Prediction by Using Delay Coordinate Embedding, in: Weigend A.S., Gershenfeld N.A. (Eds.), Proc. XV SFI Studies in the Science of Complexity, Time Series Prediction: Forecasting the Future and Understanding the Past. New York: Addison–Wesley, p. 175

Serre T., Kolláth Z., Buchler J.R., 1996a and b, A&A 311, 833 and 845

Serre T., Nesme–Ribes E., 1997, The Evolution of the Solar Cycle, in: Cini C., Provenzale A. (Eds.), Proc. International School of Physics 'Enrico Fermi' course CXXXIII, Solar Variability: Simple Models and Proxy Data, Varenna

Sokoloff D., Nesme–Ribes E., 1994, A&A 288, 293

Sonnet C.P., 1992, The Present Status of Understanding the Long–Period Spectrum of Radiocarbon, in: Taylor R.E., Long A., Kra R.S. (Eds.), Radiocarbon After Four Decades: An Interdisciplinary Perspective. New York: Springer, p. 50

Spiegel E.A., 1997, The Chaotic Solar Cycle, in: Cini C., Provenzale A. (Eds.), Proc. International School of Physics 'Enrico Fermi' course CXXXIII, Solar Variability: Simple Models and Proxy Data, Varenna

Spiegel E.A, Wolf A.N., 1987, Chaos and the Solar Cycle, in: Buchler J.R., Eichhorn H. (Eds.), Ann. NY Acad. Sci. 497, Chaotic Phenomena in Astrophysics, p. 55

Stuiver M., Braziunas T.F., 1993, The Holocene 3, 289

Takens F., 1980, Detecting Strange Attractors in Turbulence, in: Rand D.A., Young L.S. (Eds.), lecture notes in mathematics 898, Dynamical Systems and Turbulence, New York: Springer, p. 366

Tong H., Lim K.S., 1980, J. R. Stat. Soc., Ser. B 42, 245

Weigend S., Gershenfeld N.A., 1994, The Future of Time Series: Learning and Understanding, in: Weigend A.S., Gershenfeld N.A. (Eds.), Proc. XV SFI Studies in the Science of Complexity, Time Series Prediction: Forecasting the Future and Understanding the Past. New York: Addison–Wesley, p. 1

Wilson R.C., Hudson H., 1988, Nature 332, 810

Yule G., 1927, Phil. Trans. R. Soc. London, Ser. A 226, 267